JOURNAL OF APPLIED PHYSICS VOLUME 39, NUMBER 13 DECEMBER 1968

A High-Resolution Scanning Transmission Electron Microscope*

A. V. CREWE
Enrico Fermi Institute and Department of Physics, The University of Chicago, Chicago, Illinois 60637
AND
J. WALL†
Enrico Fermi Institute and Department of Biophysics, The University of Chicago, Chicago, Illinois 60637
AND
L. M. WELTER‡
Argonne National Laboratory, Argonne, Illinois 60439
(Received 20 June 1968)

A simple scanning transmission electron microscope has been built using a field-emission electron source, a new electron gun, and one lens to produce a high-contrast picture with 30 Å resolution. The final spot size is limited by the properties of the lens, in the same manner as a conventional transmission microscope. The field-emission tip requires a pressure below 10^{-9} Torr for stable operation and can have a lifetime of several months. The intensity of the source is such that high-quality pictures can be obtained in 10 sec. Specimen contamination or damage is small, as would be expected in view of the good vacuum conditions. The theory and design of the instrument are discussed, and experimental results are shown.

1. INTRODUCTION

A conventional electron microscope produces pictures containing information about the electron-scattering properties of a specimen. There are, however, numerous other effects which occur at the same time, any of which could be used to provide picture contrast. One way to detect and display these effects is by the use of a scanning microscope in which the critical electron optics are in the probe-forming system. Detectors can then be placed close to the specimen to collect secondary electrons or photons which are produced by the electron beam in the specimen. Detectors can also be placed below the specimen in order to collect electrons which have traversed it and suffered scattering or energy loss.

The history, principle of operation, and some applications of scanning microscopes have been summarized by Oatley, Nixon, and Pease,[1] and the optical principles involved in forming small electron probes have been discussed by Mulvey.[2] A small electron probe is scanned across the specimen in a television-type raster, and the information signal derived from the specimen is used to intensity modulate the screen of a synchronously scanned display tube. The signal is usually obtained by detecting either secondary electrons which can yield information on surface topography[1,3–5] or characteristic x-rays which can provide information on the distribution of elements in the specimen.[6–12]

Pease and Nixon[13] have reported the highest resolution, using a scanning microscope with a 50 Å probe and a resolution with secondary electrons of 100 Å. Their results agreed with the theoretical limits for the smallest attainable probe diameter d (Å) using a source current density J_c (A/cm²), a probe current i (A), a cathode temperature T (°K), an aperture aberration coefficient C_s (Å) in the final lens, and the electron wavelength λ (Å) as follows [their Eq. (3)]:

$$d=1.29C_s^{1/4}\lambda^{3/4}(1+7.92iT\times10^9/J_c)^{3/8}. \quad (1)$$

Typical values for a probe size of approximately 70 Å are: $J_c=10$ A/cm², $C_s=20$ cm, $T=3000$°K, $i=10^{-12}$ A, and $V=15$ kV. The best value for d is limited by the relatively large aperture aberration coefficient of a long focal length lens, the value of the current density available in a thermionic source, and the minimum value of probe current needed to form a reasonably noise-free picture in a nominal recording time of a few minutes. A long focal length is needed in order to keep the specimen out of the high magnetic field of the final lens to allow the efficient collection of secondary electrons.[13] The image contrast is determined by the num-

* Work performed under the auspices of the U.S. Atomic Energy Commission.
† Supported by U.S. PHF Training Grant GM-780.
‡ New address: Ultek Division, Perkin-Elmer Corporation, Palo Alto, Calif.

[1] C. W. Oatley, W. C. Nixon, and R. F. W. Pease, Advan. Electron. Electron Phys. **21**, 181 (1965).
[2] T. Mulvey, in *Focusing of Charged Particles*, A. Septier, Ed. (Academic Press Inc., New York, 1967), Vol. 1, Chap. 2, p. 469.
[3] K. C. A. Smith and C. W. Oatley, Brit. J. Appl. Phys. **6**, 391 (1955).
[4] T. E. Everhart, O. C. Wells, and C. W. Oatley, J. Electron. Control **7**, 97 (1959).
[5] R. F. W. Pease, IEEE Spectrum **96** (October 1967).
[6] H. H. Pattee, Jr., J. Opt. Soc. Am. **43**, 61 (1953).
[7] H. H. Pattee, Jr., *X-Ray Microscopy and Microradiography* (Cambridge University Press, Cambridge, England, 1956), p. 367.
[8] P. Duncumb and V. E. Cosslett, *X-Ray Microscopy and Microradiography* (Cambridge University Press, Cambridge, England, 1956), p. 374.
[9] P. Duncumb, Brit. J. Appl. Phys. **10**, 420 (1959).
[10] V. E. Cosslett and W. C. Nixon, *X-Ray Microscopy* (Cambridge University Press, Cambridge, England, 1960), Chap. 1, p. 9, and Chap. 7, p. 202.
[11] R. M. Dolby, *X-Ray Optics and X-Ray Microanalysis* (Stanford University, Calif., 1963), p. 483.
[12] I. W. Bronshtein and B. S. Fraiman, Sov. Phys.—Solid State **3**, 2337 (1962).
[13] R. F. W. Pease and W. C. Nixon, J. Sci. Instr. **42**, 81 (1965).

ber of collected electrons per picture element compared to the effect of shot noise,[8] and the maximum picture recording time is limited by electrical and mechanical instabilities. These considerations set a lower limit to the usable current of 10^{-12} A. A hot filament cannot deliver this current through the small aperture required for high resolution, so the aperture size must be chosen as a compromise between resolution and contrast. The difference between probe size and resolution is probably due to secondaries which are produced at some depth below the surface. This difference is even greater when x-rays are used to produce picture contrast.

2. NEW MICROSCOPE DESIGN

The scanning microscope described here uses a field-emission tungsten tip as the source of electrons. Such sources are smaller and brighter than thermionic sources and therefore should be capable of providing smaller useful probe sizes. It is apparent from the previous discussion, however, that a different contrast mechanism should be used if one wants to take advantage of a smaller probe size. Electrons which are transmitted through the specimen were used in this work and, in particular, an energy selecting system was included so that inelastic as well as elastic scattering information could be used.[14,15]

2.1. Source Size and Brightness

A conventional hot filament has a maximum brightness corresponding to a current density J_c, which is limited by the evaporation rate of the filament at high temperature and by space charge. This maximum value of J_c sets a limit on the minimum diameter of the final probe [see Eq. (1)]. Since the hot filament must operate at a high temperature, a second disadvantage of this source is the large energy spread for the emitted electrons (typically 0.9 eV)[16] which can limit the minimum probe diameter, especially at low accelerating voltages, and which does limit the energy resolution for specimen characteristic energy-loss analysis.[14,17–19]

A field-emission tungsten tip should provide some improvement because it provides: (a) more than a thousand times increase in brightness over a hot filament source,[20] (b) operation at room temperature which gives a measured energy spread as low as 0.192 eV,[21,22] and (c) an effective source diameter of about 30 Å. A disadvantage of using the field-emission tip is that a pressure of about 10^{-9} Torr is needed for stable operation. However, this pressure is attainable using commercial pumps (without baking) and is also desirable for the reduction of specimen contamination, a problem observed by Pease and Nixon at pressures above 10^{-6} Torr.[13]

2.2. New Electron Gun

A new gun which not only accelerates the electrons from the tip, but also refocuses them into a small spot, has been reported and only the results are summarized here.[14,20,23] A cross section of the gun, which is cylindrically symmetric, is shown in Fig. 1. The performance of the gun can be characterized by the effects of source size, aperture aberration, diffraction (full width at half maximum of the first diffraction zone), and chromatic aberration, respectively,[24,25]

$$D_s = 2mr \tag{2}$$

$$D_a = \tfrac{1}{2}C_s m^4 \alpha_0^3 (V_0/V_1)^{3/2} \tag{3}$$

$$D_d = 0.61(\lambda_0/\alpha_0) \tag{4}$$

$$D_c = 2C_c\alpha_0\Delta(V_0/V_1) = 2C_c\alpha_0\{(\Delta V/V_1)[(V_0/V_1)-1]\} \tag{5}$$

$$I_{\text{beam}} = I_{\text{tip}}\alpha_0^2 m^2 (V_0/V_1), \tag{6}$$

where m is the gun magnification, r is the apparent source radius of the tip,[20] C_s is the aperture aberration coefficient (referred to object space), λ_0 is the wavelength of an electron with energy eV_0, C_c is the chromatic aberration coefficient (referred to image space) which is written in units of cm per change in ratio

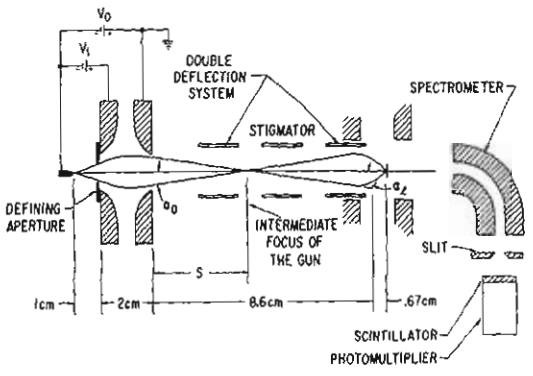

FIG. 1. Ray diagram for the new scanning transmission microscope where V_1 is the voltage applied from tip to 1st anode, V_0 is the accelerating voltage applied from tip to 2nd anode, α_0 is the beam half-angle at the exit of the gun, α_i is the beam half-angle at the exit of the auxiliary lens, and S is the position focus measured from the exit of the gun.

[14] A. V. Crewe, Science **154**, 729 (1966).
[15] A. V. Crewe, *Proceedings of the 6th International Congress for Electron Microscopy, Kyoto* (Maruzen Co., Ltd., Tokyo, 1966), p. 625.
[16] Möllenstadt and Duker, Z. Naturforsch. **89**, 89 (1953).
[17] A. V. Crewe, J. Appl. Phys. **35**, 3075 (1964).
[18] H. Watanabe, Hitachi Rev. **14**, 20 (1965).
[19] S. L. Cundy, A. J. F. Metherell, and M. J. Whelan, J. Sci. Instr. **43**, 712 (1966).
[20] A. V. Crewe, D. N. Eggenberger, J. Wall, and L. M. Welter, Rev. Sci. Instr. **39**, 576 (1968).
[21] R. D. Young, Phys. Rev. **113**, 110 (1959).
[22] R. D. Young and E. W. Müller, Phys. Rev. **113**, 115 (1959).
[23] J. W. Butler, *Sixth International Congress for E. M. (Kyoto)*, 191 (1966).
[24] Note that the effect of chromatic aberration was neglected in the previous report (Ref. 20) and that the coefficient of aperture aberration C_s reported therein is a factor of four low.
[25] See Ref. 2, Chap. 2, p. 476.

$\pm\Delta(V_0/V_1)$, $\pm e\Delta V$ is the energy spread for electrons emitted from the tip, and V_0, V_1, α_0, and S are defined in Fig. 1. The beam current is calculated assuming the tip current is emitted into 1 sr. The lens parameters and image diameter D for the gun are plotted as a function of the voltage ratio (V_0/V_1) in Fig. 2, where D is obtained by adding the aberration diameters [Eqs. (2)–(5)] in quadrature[25] and each optimum α_0 is found by setting the diffraction term equal to the sum of the chromatic and aperture aberration terms.

2.3. Auxiliary Lens

A single auxiliary lens is used in order to demagnify the image produced by the gun. The addition of this lens modifies Eqs. (2)–(5) as follows:

$$d_s = 2mm_l r \tag{2a}$$

$$d_a = \tfrac{1}{2}C_s m^4 m_l^4 \alpha_l^3 (V_0/V_1)^{3/2} \tag{3a}$$

$$d_d = 0.61(\lambda_0/\alpha_l) \tag{4a}$$

$$d_c = 2C_c \alpha_l m_l^2 \Delta(V_0/V_1) \tag{5a}$$

$$I_{\text{beam}} = I_{\text{tip}} \alpha_l^2 m^2 m_l^2 (V_0/V_1), \tag{6a}$$

where the d terms represent spot diameters in the final image plane, m_l is the magnification of the auxiliary lens, α_l is the beam half-angle at the exit from the auxiliary lens, and all other terms are as previously defined. The solenoidal lens also introduces two new aberration terms,[26] the aperture aberration effect

$$d_a' = \tfrac{1}{2}C_s' \alpha_l^3 \tag{7}$$

and the chromatic aberration effect

$$d_c' = 2\alpha_l C_c' \Delta V/V_0, \tag{8}$$

where the prime indicates that the quantities refer to the solenoidal lens.

All of the results given here have been obtained using a standard RCA intermediate lens[27] packaged in a vacuum-tight enclosure (see Fig. 3). Although this lens is an intermediate type and therefore is not of "objective" quality, it was conveniently adaptable to existing geometry. The theoretical parameters[28,29] for this lens are a chromatic aberration coefficient $C_c'=0.51$ cm, an aperture aberration coefficient $C_s'=0.71$ cm, a focal length $f_0=0.67$ cm, and the required ampere turns $NI=9.2(V_0)^{1/2}$. Some water cooling was provided by wrapping two turns of copper tubing around the lens enclosure.

A typical set of operating conditions is $V_0/V_1=17$, $V_1=1000$ V, 50 μ aperture in the 1st anode: $m=1.27$, $m_l=0.084$, $\alpha_l=5.6\times10^{-3}$, $\Delta V=\pm0.1$ V, $I_{\text{tip}}=10^{-5}$ A,

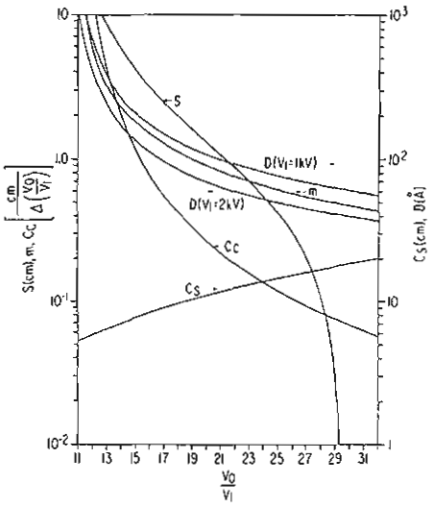

FIG. 2. Summary of lens parameters and image diameter (D) for the new electron gun having the geometry shown in Fig. 1. The value of D is given for two different tip-to-1st-anode voltages ($V_1=1$ kV and $V_1=2$ kV).

which gives $d_s=3.2$ Å, $d_a=0.7$ Å, $d_d=10.4$ Å, $d_c=5.6$ Å, $d_a'=6.2$ Å, $d_c'=3.3$ Å, $d_{\text{rms}}=14$ Å, and $I_{\text{beam}}=6.1\times10^{-11}$ A. Reducing m_l (keeping α_l constant) reduces the effect of gun aberrations and source size while sacrificing beam current. In the limit, only d_d [Eq. (4a)], d_a' [Eq. (7)], and d_c' [Eq. (8)] are significant. These terms give the same ultimate resolution as one would calculate for a conventional microscope using the same lens. In the above example this limit is 12.1 Å.

2.4. Scanning System and Astigmatism Correction

The scanning arrangement is similar to that described by Oatley *et al.*,[1] and consists of two magnetic deflection systems (see Fig. 3). The deflector uses four coils of wire, each forming the perimeter of the outer surface of a hollow cylinder divided into quadrants (see Fig. 4). Each coil consists of one turn of teflon-covered wire, and the diametrically opposite coils are wound in series with interconnections routed to cancel the unwanted fields. The reasons for using a double-deflection arrangement are to permit the beam to always pass through the center of the auxiliary lens[1] and to make the size of the raster on the specimen (picture magnification) independent of the axial position assumed by the intermediate image. A push–pull current signal with a 3 A peak and sawtooth shape is applied to the coils to generate deflection fields which provide a maximum field of view of 100 μ. A raster time of 1 sec is typically used for focusing, and a 10 sec raster is used when photographing the image. Manual control of direct current through the deflection coils provides the equivalent of a vernier specimen position control.[30]

[25] C. E. Hall, *Introduction to Electron Microscopy* (McGraw-Hill Book Co., New York, 1953), Chap. 6, p. 116.

[27] We are indebted to J. Reisner (RCA, Camden, N.J.), who permitted us to use this lens.

[28] G. Liebmann and E. M. Grad, Proc. Phys. Soc. (London) **B64**, 956 (1951).

[29] P. Durandeau and C. Fert, Rev. Opt. **36**, 205 (1957).

[30] Actually the position of the raster on the specimen, rather than the specimen itself, is being moved.

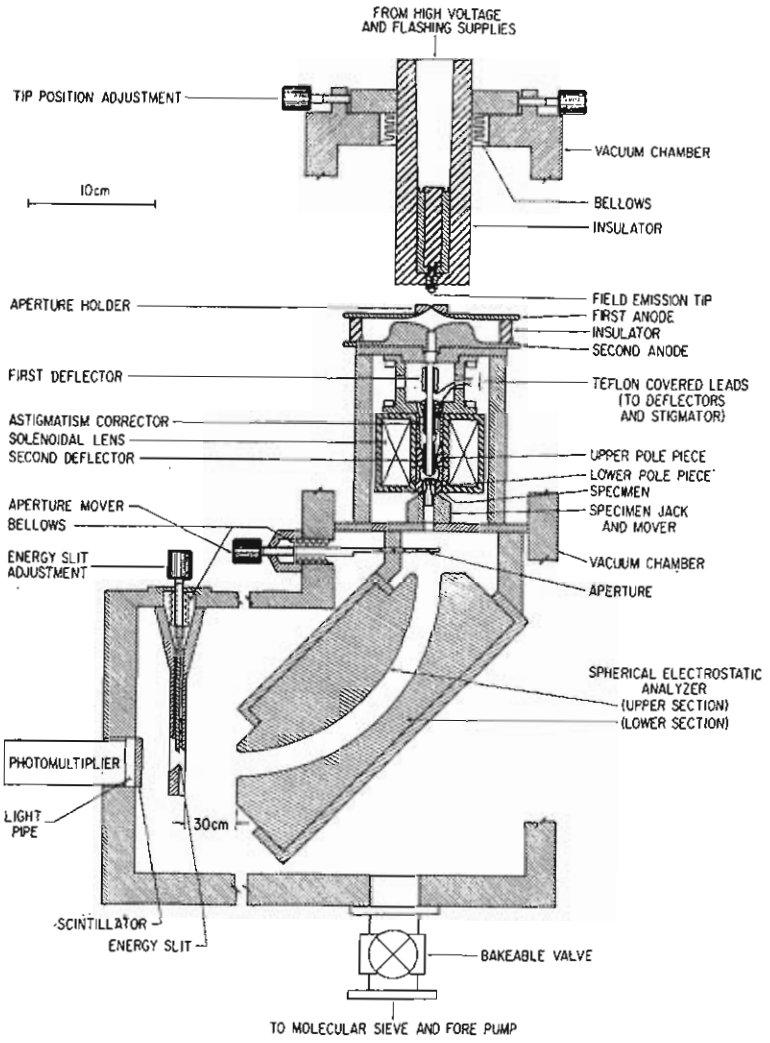

FIG. 3. Cross section of the experimental scanning electron microscope.

The correction of astigmatism is accomplished electrically, using Rang's technique[31] involving two quadrupoles, one rotated by 45° with respect to the other. This device provides independent magnitude and angle control of the correcting field. A sine–cosine potentiometer is used to provide appropriate signals for the electrical rotation. The coils for the astigmatism corrector are wound in octants to provide eight poles, four for each quadrupole. Proper wire routing again makes it possible to wind the four coils for a given quadrupole in series (see Fig. 4).

2.5. Information Detection and Readout

After traversing the specimen, the electrons pass through a variable aperture and then through an electrostatic energy analyzer. Image contrast is therefore controlled by adjusting the aperture (scattering contrast) or by adjusting the voltage on the spectrometer (energy-loss contrast). In principle it is also possible to obtain a display of a diffraction pattern by scanning the transmitted electrons across the aperture and using parallel illumination of the specimen. Finally, the electrons are detected by means of a scintillator and photomultiplier (Fig. 3).

The information signal detected by the scintillator is used to modulate the intensity of a synchronously scanned storage tube.[32] Although the image of the specimen can be photographed directly on the storage-tube screen, a parallel system consisting of a high-

FIG. 4. The magnetic double-deflection and astigmatism corrector. The right-hand winding is the 1st deflector, the left-hand winding is the 2nd deflector, and the center winding is the astigmatism corrector.

[31] O. Rang, Optik 5, 518 (1949).

[32] W. K. Brookshier and J. Gilroy, Trans. Nucl. Sci. IEEE, NS-12, 104 (1965).

resolution cathode ray tube and a permanently mounted camera has been found to be more convenient. The storage tube is more useful for focusing the microscope. Since the information signal is available for electronic processing, it is readily adaptable to computer analysis of specimen information. A simple example of electronic signal processing is given in a later section of this report.

2.6. Power Supply Stability

The final spot size can be undesirably increased by instabilities in the magnetic lens current and in the high voltages.[33] The resolution is further affected by instabilities which cause the probe position to vary in an undesired manner such as by ripple on the scanning signals. All pertinent power supplies were required to have equivalent ripples of less than a few angstroms and equivalent instabilities of less than a few angstroms of probe-position drift per hour. These requirements correspond to voltage and current ripples of 0.1 V and 1 μA, respectively, and stabilities of about 3 ppm/h. An additional reason for using a high-voltage supply with low ripple with this microscope is to allow an energy resolution for the electrostatic analyzer of about 0.2 eV, a figure which is limited by the electron energy spread from the field emission tip.

A commercially available high voltage supply[34] and variable current supply[35] have been successfully used in practice. However, only beam and leakage currents (which are less than 0.03 μA) are drawn from the high-voltage supply with this microscope, and a low power system has been designed which more than meets the stability and ripple requirements mentioned above. A raster generator and scan amplifiers have also been designed which meet these same requirements. Further details of the power supplies which are used to operate the gun can be found in Ref. 20.

3. EXPERIMENTAL RESULTS

The performance of the microscope, as a function of the various parameters, depends upon the position of the defining aperture in the probe-forming elements. We have used several different positions for this aperture, but the experimental results will be given for the system where the aperture is placed on top of the first anode (Fig. 1). By defining the beam half-angle at this point, a small tip movement can be used to position the beam on the electron-optical axis of the solenoidal lens, and any resulting off-axis aberration in the gun will at least be demagnified by the solenoidal lens. Equations (2a)–(7) were used to calculate the resolution and these results are plotted in Fig. 5 for three different aperture sizes, 50, 100, and 200 μ.

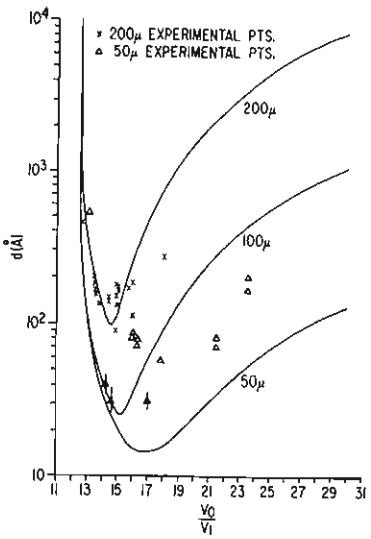

FIG. 5. Theoretical and experimental data for the geometry shown in Fig. 1. The bar through the triangle indicates typical measurements obtained with the 50 μ aperture after aligning the system electron-optically.

The experimental results which are also given in Fig. 5 show some divergence from the theoretical values, but perhaps no more than would be expected. They represent various tungsten tips and various voltages and lens currents. In particular, they represent various methods used to align the electron-optical system.

The best alignment system which was used is as follows. First the field emission source is placed on the axis of the gun. This is done by turning off the auxiliary lens and using the electron gun to focus on the specimen. Alignment is achieved when a variation in tip voltage only causes defocusing and does not produce an image displacement. Then the lens is turned on and the electron beam is centered in the lens, using dc currents in the two deflection systems. The criterion for centering is that the raster rotates about a fixed point on the specimen as the lens current is changed. In order to meet this criterion the beam must be located within 20 μ of the axis.

Using this technique we obtained a best resolution of 30 Å and consistently achieved a resolution better than 100 Å. Many of the experimental points which are shown were obtained before this alignment technique was developed, and therefore disagreement with the theoretical curves may be expected. These points were included in Fig. 5 in order to demonstrate agreement with the trend of the theoretical curves.

The micrographs included in this section were obtained using the arrangement shown in Fig. 3, and using the alignment criteria discussed in the last section.

A thin aluminum specimen ($\approx$1000 Å thick) was evaporated on a NaCl substrate. The salt was dissolved away in distilled water, and the aluminum was picked up on a grid. A micrograph of this specimen is shown in Fig. 6(a). The best resolution obtained with this

[33] V. K. Zworykin, G. A. Morton, E. G. Ramberg, J. Hillier, and A. W. Vance, *Electron Optics and Electron Microscope* (John Wiley & Sons, Inc., New York, 1945), Chap. 6, p. 213.

[34] Canal model 80 kV, Canal Industrial Corp., 4935 Cordell Ave., Bethesda 14, Md.

[35] Model TC-602CR, Princeton Applied Research Corp., P.O. Box 565, Princeton, New Jersey.

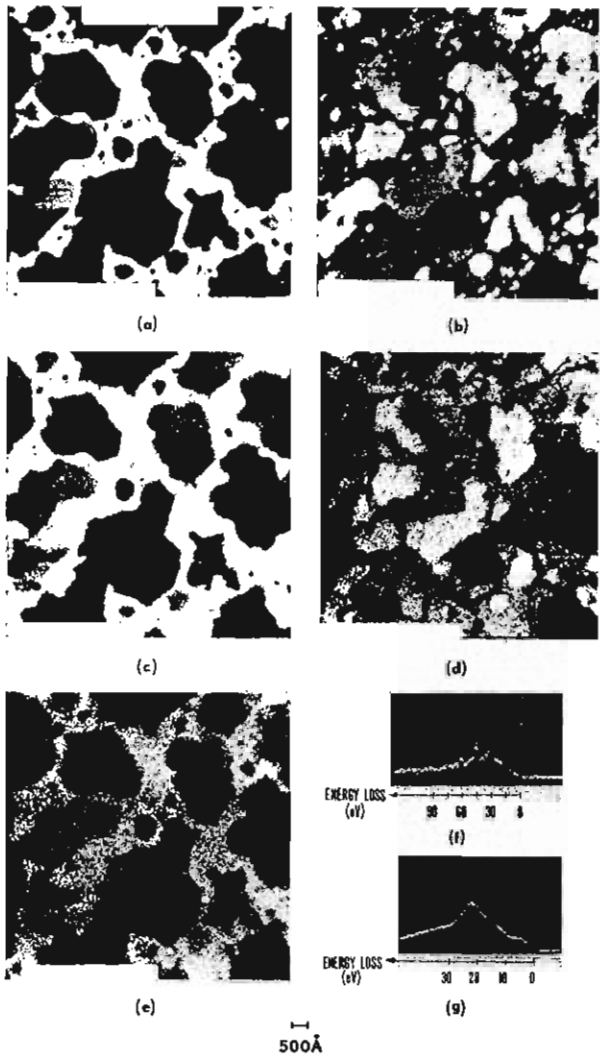

FIG. 6. Micrographs of a thin evaporated aluminum specimen. Figure 6(a) is a micrograph taken with zero-energy-loss electrons, while (b), (c), (d), and (e) are micrographs taken with an energy loss of 15, 22, 30, and 35 V, repectively. Figure 6(a) corresponds to the kind of picture which would be obtained in a conventional electron microscope. (f) and (g) show energy-loss data taken while the electron probe was stationary. Figure 6(f) was taken on a black area of the specimen and the curve indicates substantially pure aluminum. The peaks are the plasma-loss peaks which occur at 15, 30, 45, and 60 V. Figure 6(g) was taken with the electron probe stationary on a white area and indicates that this is probably aluminum oxide.

system was about 30 Å. This figure was determined by finding the smallest reproducible feature on the pictures and also by measuring the risetime of the current in the detector when the probe was repeatedly scanned across a sharp edge in the specimen. The small horizontal variations were caused by mechanical vibrations, and were reduced to the present magnitude by decoupling the specimen from its holder using a small spring, which forced the specimen against a surface fixed to the pole piece of the lens. Figure 6(b)–6(e) shows a series of pictures taken of the same aluminum specimen using various energies in the transmitted beam. At zero energy loss [Fig. 6(a)] the picture corresponds to similar ones obtained in a conventional electron microscope. Using electrons which have lost 15 V (corresponding to the first plasma loss) the picture is quite different [see Fig. 6(b)]. The light areas on this picture can be presumed to be aluminum because the first plasma loss is very pronounced.

At 22 V loss the light areas on the picture represent something other than aluminum because pure aluminum transmits almost no electrons which have lost 22 V [see Fig. 6(c)]. However, contaminating materials (such as aluminum oxide or residual salt) may produce such losses. At 30 V loss the aluminum again appears light because of the dominance of the second plasma loss. It can be seen that at 15 and 30 V loss one sees the aluminum underneath an overlying layer of contamination.

Figure 6 also shows energy-loss curves taken while the electron probe was stationary, first on a black area (zero loss) and then on a white area. While no exact analysis can be performed, the curve taken on the white area could be aluminum oxide [Fig. 6(g)], while the one taken on the black area is certainly aluminum [Fig. 6(f)].

Figure 7 is a micrograph of a biological specimen, in this case *Helix Aspersa* (snail sperm tails) which has been embedded in Epon and sectioned to about 500 Å in thickness. Two pictures are shown, one using a signal direct from the photomultiplier and the other using a differential signal. The differentiation technique is a simple form of electronic signal processing which, in this case, accentuates the features of the micrograph on a uniform background, giving an effect similar to shadowing.

Figure 8 is of the same specimen, but at larger magnification. The lines are known to be 100 Å apart.

The magnification of the microscope was verified many times, and the crossed replica grating with 4630 Å spacing shown in Fig. 9 is an example of a specimen used for calibration.

Each micrograph was taken with a Polaroid camera on a high-resolution cathode ray tube using a 10 sec raster. The accelerating voltage was usually between 10 and 30 kV, and the specimen current varied from 10^{-12} to 10^{-9} A. Typically, no specimen contamination was observed, although one exception was a formvar substrate which outgassed so severely that contamination did occur, presumably caused by a large pressure differential in the specimen area with respect to the chamber. "Negative contamination" has been observed immediately after putting a specimen into the vacuum. This phenomena appears to be a sublimation of some of the substrate constituents, probably water vapor, but has been reduced by putting the specimens in a vacuum of 10^{-8} Torr for a few hours before placing them in the microscope. Although "negative contamination" has, at times, been observed on the substrate, no change in actual specimen detail (to resolutions below 50 Å) has been detected, even though these specimens have often been in the vacuum for months.

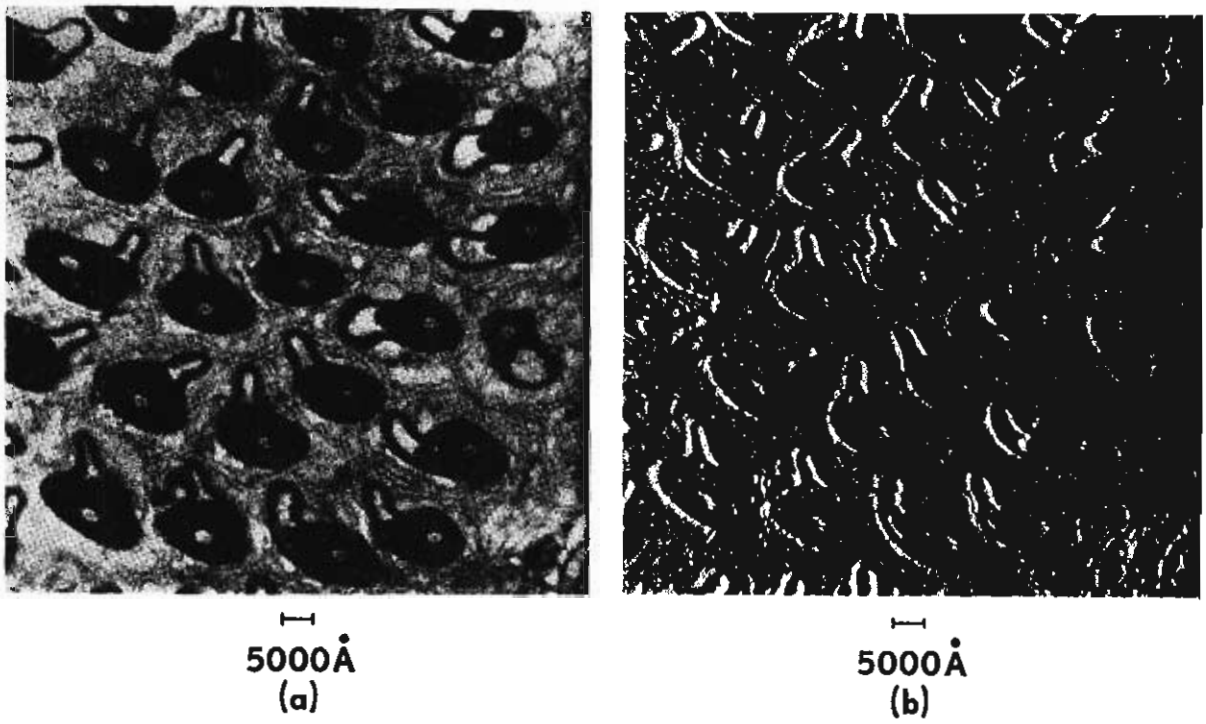

FIG. 7. (a) Typical micrograph of sectioned *Helix Aspersa*. (b) The same specimen area as shown in (a), but using a differentiated signal.

The use of a field emission tip as an electron source has, in the past, often been rejected for two reasons: the low pressure needed to provide reasonable tip life and the instability of the tip as an electron source, especially if operated above about 10^{-11} Torr. This microscope operates at a vacuum of about 10^{-9} Torr, which apparently does not affect many specimens, and which does not cause the stability of the field emission source to be intolerable. Typically, tip lifetimes of many months are being experienced. The most frequent source of tip troubles is the occurrence of a discharge between the two anodes, and the transient usually destroys the tip. Periodic flashing or reconditioning of the tip[20] is required at intervals of a few minutes to several hours, depending on the pressure. Even when the beam intensity does change for an instant during the raster, interpretation of the micrograph is not seriously hindered. A disadvantage of the required low operating pressure is that about 3 h are now needed to attain the appropriate vacuum after a

FIG. 8. A higher magnification of the wheel-like center section of a typical *Helix Aspersa*. The radial lines are known to be about 100 Å apart.

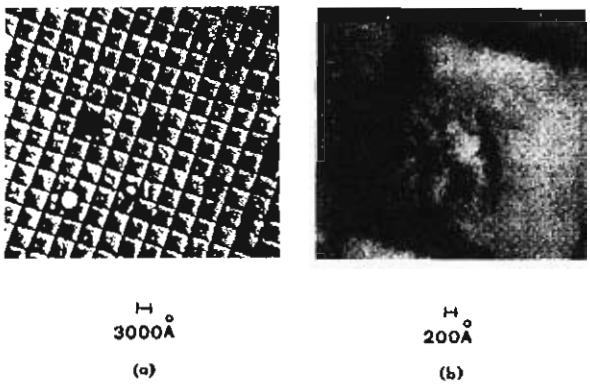

FIG. 9. A crossed replica grating with 4630 Å spacing shown at two different magnifications.

specimen change is made; however, construction is underway on a specimen changer which should reduce this cycle time to about 10 min.

ACKNOWLEDGMENTS

The authors wish to express their gratitude to M. Isaacson and D. Johnson for their invaluable assistance in this work and to Dr. J. Gilroy and D. N. Eggenberger of the Electronics Division of Argonne National Laboratory for their help and hospitality. In addition we are greatly indebted to the Central Shops at Argonne who fabricated this instrument. Finally, we would like to thank Dr. John Reisner of R.C.A. for his help with the magnetic lens.

JOURNAL OF APPLIED PHYSICS VOLUME 39, NUMBER 13 DECEMBER 1968

Factors Influencing the Acoustic Properties of Vitreous Silica

DAVID B. FRASER

Bell Telephone Laboratories, Incorporated, Murray Hill, New Jersey 07974

(Received 18 June 1968; in final form 12 August 1968)

The acoustic properties of various types of commercial vitreous silica have been studied as functions of thermal treatment and impurity-ion concentrations. The properties studied include density, shear-wave attenuation, shear and dilatational wave velocities, and elastic constants. The measurements of acoustic properties are made on small sphere-shaped samples using primarily a technique that sets the sphere into a resonant mode of vibration and then allows the vibration to decay freely. Both frequency and the decrement of the decay are measured. Use of this resonant sphere technique is particularly appropriate to the present study because it permits precise measurements on samples small enough to conveniently undergo laboratory modification, and it permits the study of velocity variations in a single block of material by measurements on many localized samples. The major findings of this study are the following: (1) An increase of one degree in fictive temperature (a parameter assumed to be related to the equilibrium internal configuration of the glass) causes a decrease in the shear velocity of 13–16 ppm. (2) Gross differences of OH content result in differences in shear velocity. Although shear velocity differences could be induced by changing fictive temperature and the gross OH content, shear velocity fluctuations (of the order ± 125 ppm) observed in single large pieces of commercial vitreous silica were not correlated with variation of either fictive temperature or OH content. Attempts to relate fluctuations of shear velocity to differences of Na content were inconclusive.

I. INTRODUCTION

Vitreous silica finds wide application in ultrasonic delay lines because of its very low acoustic loss and high degree of elastic isotropy. Recent measurements[1] have shown that small velocity fluctuations occur in large pieces of the material which may degrade the performance of finished delay lines. This behavior has been found in all types of vitreous silica, including fused natural quartz[2] of both medium and low OH content and fused silica[2] made by the hydrolysis of $SiCl_4$ in an oxygen–hydrogen burner. In the past, two factors have been tentatively identified as significantly influencing the physical properties (especially optical properties); these are the thermal history and the OH ion concentration. The work reported in this paper has two objectives:

(1) To discover the important factors influencing the acoustic properties of vitreous silica for delay line applications.

(2) To show that acoustic measurements can be made with sufficient precision to reveal features of the fundamental structural behavior of vitreous silica not discernible by other techniques.

Related studies of vitreous silica utilizing pulse-echo techniques have been carried out at these Laboratories by Krause[3,4] and Papadakis.[5] Krause compared the low-temperature and the room-temperature acoustic properties of a number of vitreous silica specimens produced by Amersil and presented some evidence that property variation among the silicas was due to differences in thermal history and OH content. Papadakis has studied homogeneity of pieces of vitreous silica up to 40 cm in dimension and has related some of the velocity variations to visible defects. The present investigation has utilized the resonant sphere technique[6] to study samples of vitreous silica which are representative of the types currently produced.

The resonant sphere technique offers certain advantages over other methods of acoustic study. Since

---

[1] D. B. Fraser, J. T. Krause, and A. H. Meitzler, Appl. Phys. Letters **11**, 308 (1967).

[2] Terminology has been somewhat confusing with respect to vitreous silica. In accord with a practice that has been receiving increasing acceptance, the term fused quartz will designate a fused natural material and the term fused silica will designate a synthesized vitreous silica.

[3] J. T. Krause, unpublished comparison of several Amersil vitreous silicas and specially prepared vitreous silicas.

[4] J. T. Krause, J. Am. Ceram. Soc. **47**, 103 (1964).

[5] E. P. Papadakis (unpublished).

[6] D. B. Fraser and R. C. LeCraw, Rev. Sci. Instr. **35**, 1113 (1964).